Imaging along conformal curves

Huanyang Chen*

Institute of Electromagnetics and Acoustics and Department of Electronic Science, Xiamen University, Xiamen 361005, China

(Received 5 July 2018; published 22 October 2018)

In this article, we prove that conformal transformation optics could be used to construct absolute instruments. The Mikaelian lens, whose refractive index profile is $1/\cosh(x)$ [A. Mikaelian and A. Prokhorov, Progress in Optics **17**, 279 (1980)], are of imaging functionalities along lines and will be used as a generic lens. Under a conformal mapping, it can be transformed to another lens, where imaging or self-imaging happens along predesigned curves. Ray tracing simulations are performed to confirm the imaging functionalities.

DOI: 10.1103/PhysRevA.98.043843

Absolute instruments are a very special type of lenses, where any source in them will induce images or self-images with no aberration [1–4]. The famous ones are Luneberg lens, Eaton lens, and Maxwell's fish-eye lens [5–7]. They have many applications in antenna designs [8], lensing systems [9], and cloaking designs [4,10]. They are usually of rotation symmetry, and have been related to special curved surfaces, which were called geodesic lenses [11,12]. Recently, another type of absolute instruments was proposed without rotation symmetry by employing analogy between geometrical optics and classical mechanics based on the Hamilton-Jacobi equation [13], which is the second example of such kinds after the Lissajous lens [14]. The absolute instruments cannot be designed directly from transformation optics (TO), which is an important technique in controlling the rays and waves arbitrarily [10,15–17]. Nevertheless, TO combining with such lenses does bring about many important achievements, such as transmuted Eaton lens [18] and flattened Luneberg lens [19]. More recently, another important lens, the Mikaelian lens, has been recalled [3,20]. Its refractive index profile is $1/\cosh(x)$ and are of imaging functionalities along lines. Originally, people use it to design self-imaging waveguides. Now, it has been shown to link with the famous Maxwell's fish-eye lens by a simple conformal mapping. Such a lens was implemented in optical frequencies and demonstrated additional interesting effect, the Talbol effect [21].

It is very interesting that, although the Mikaelian lens is not an absolute instrument, by performing a conformal mapping it becomes one. Can we use the Mikaelian lens as a kernel and produce other lenses with similar imaging functionalities? If yes, conformal transformation optics will become another technique to construct such lenses. In this article, we will simply start from the connection between the Mikaelian lens and Maxwell's fish-eye lens. Later on, by scaling the Mikaelian lens, we found several interesting imaging effects along circles, which were overlooked by the community when studying the properties of generalized Maxwell's fish-eye lens. Finally, we outline two examples based on two conformal mappings, which are usually used to produce bipolar coordinates and elliptic coordinates. All the imaging functionalities will be confirmed by ray tracing simulation from commercial software COMSOL.

Let us start from a conformal mapping of $w = w(z) = u + iv$ or $z = z(w) = x + iy$. Under the mapping, the refractive index profile in z space and that in w space have the following relationship [4,10]:

$$n_z = n_w \left| \frac{dw}{dz} \right|. \tag{1}$$

If $n_w = \frac{1}{\cosh(mu)}$, under the mapping of $z = \exp(w)$ [with $x = \exp(u)\cos v$ and $y = \exp(u)\sin v$], or $w = \ln(z)$, the refractive index profile in z space can be written as [3,21]

$$n_z = \frac{2r^{m-1}}{1 + r^{2m}}, \tag{2}$$

which is simply a generalized Maxwell's fish-eye lens (where $r = \sqrt{x^2 + y^2}$). The profile in w space is a Mikaelian lens [20], which has recently been realized in optical frequencies [21]. It has a very interesting property that any source at an arbitrary point (u_0, v_0) will induce images along $u = \pm u_0$ [21]. The parameter m is to scale the period of the images. Fig. 1(a) shows the ray tracing simulation for the source at (2, -8), and it cause images at $(2, -8 + 2n\pi)$ along $u = 2$ (in green and solid format) and $[-2, -8 + (2n + 1)\pi]$ along $u = -2$ (in red and dashed format). Here n is an integer and $m = 1$. We also plot the refractive index profile together in Fig. 1(a), where $n_w = 1$ for $u = 0$, and 0 for u goes to infinity. Under the above conformal mapping, it goes back to the famous Maxwell's fish-eye lens [7], whose refractive index profile is plotted in Fig. 1(b) with $n_z = 2$ at the origin and 0 for r goes to infinity. If we put a source at (2, 0), it will have a perfect image at $(-1/2, 0)$ and then a self-image at (2, 0). All the light trajectories are circles, which are mapped simply from a period of those in Mikaelian lens. If $m < 1$, e.g., $m = 1/2$, the light trajectories will travel around the origin twice (or $1/m$ times, for other m) before it comes back as a self-image. We then put a source at (2, 0), it causes a perfect image at $(1/2, 0)$ and a self-image at (2, 0), as shown in Fig. 1(c). Two periods of the light trajectories around the origin are related to a period of those in Mikaelian lens, and are no longer circles.

*kenyon@xmu.edu.cn

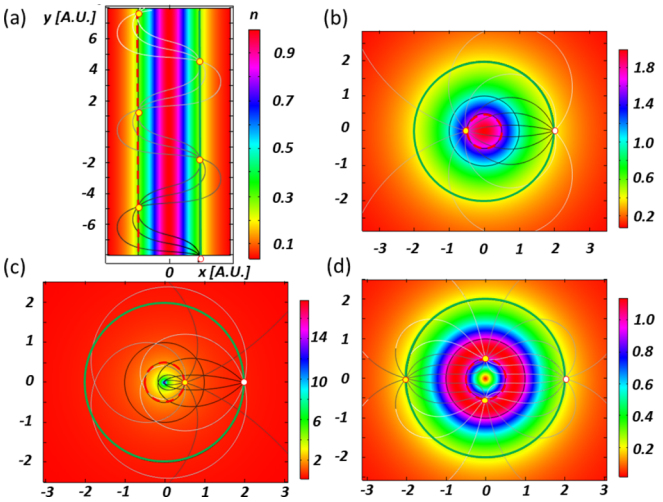

FIG. 1. The ray trajectories and refractive index profiles for (a) a Mikaelian lens, (b) a Maxwell's fish-eye lens, and a generalized Maxwell's fish-eye lens with (c) $m = 1/2$ and (d) $m = 2$. The white points are the sources while the yellow points are images. The solid circles in green are mapped from the solid line in green, while the dashed circles in red are mapped from the dashed line in red. The color of the ray trajectories changing from black to gray and to white denotes the propagation of time. We use arbitrary units [a.u.] for x and y coordinates.

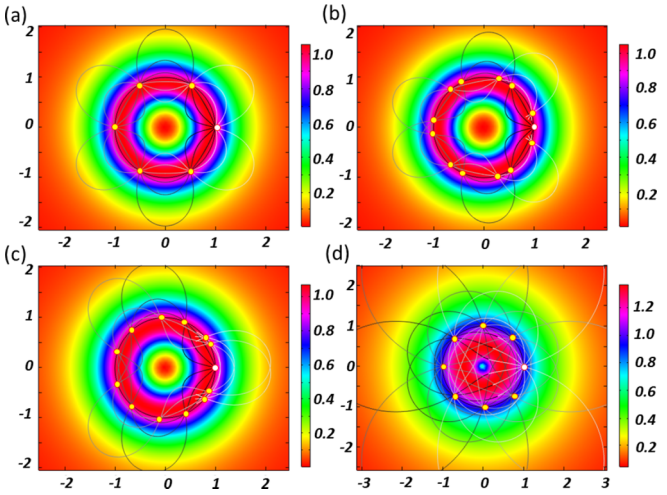

FIG. 2. The ray trajectories and refractive index profiles for a generalized Maxwell's fish-eye lens with (a) $m = 3$, (b) $m = \pi$, (c) $m = e$, and (d) $m = 4/3$. The white points are the sources while the yellow points are images.

The refractive index profile is plotted as well, with a singular infinity at the origin. Such a lens has been well studied [3,11]. However, for $m > 1$, it is still not very clear. But with the help of Mikaelian lens, we can understand the effect very well. In Fig. 1(d), we plot the refractive index profile for $m = 2$, with the maximum value near $r = 1$. If we put a source at (2, 0), it will cause images at (0, 1/2), (−2, 0), and (0, −1/2), and a self-image. The light trajectories are related to two periods of those in Mikaelian lens. Note that for the above three cases of Maxwell's fish-eye lenses, the source and images are located at $r = \exp(u)$ or $\exp(-u)$. For $u = 0$, $r = 1$, the two sets of images will be simply mapped to the unit circle.

Now we come to study another intriguing effect for such a lens for $m > 1$. For simplicity, we study the imaging along the unit circles. In Fig. 2(a), we plot the refractive index profile and related light trajectories for $m = 3$. The maximum value of the index is located closer to $r = 1$ compared to that for $m = 2$ in Fig. 1(d). There are six images (or self-image) along the unit circles, for a source at (1, 0). What happens if m is no longer an integer? More interestingly, how about m is an irrational number? We then plot the light trajectories for $m = \pi$ in Fig. 2(b). It is very interesting that the imaging effect is still maintained, but the light will not come back to the source point (1, 0) (i.e., no self-imaging effect). We also plot the light trajectories for $m = e$ in Fig. 2(c), where similar effect happens. In principle, the imaging effect will happen along the unit circle forever, if there is no loss. Note that all the above three refractive index profiles are very close to each other. If m is a rational number, say M/N, there will be still self-imaging effect. However, it becomes a bit complicated. For example, we plot the light trajectories for $m = 4/3$ in Fig. 2(d). There are eight images (or self-image) along the unit circles, for a source at (1, 0). However, the light trajectories will travel around the origin three times (6π) before it comes back as a self-image.

Since the Mikaelian lens has imaging functionalities along lines, which could, in principle, be transformed to any arbitrary curves, it could be used as a generic lens under any kind of conformal mapping, and will bring about a series of interesting lenses, which is the important point of this letter. We will outline this method with two common mappings, which are used to obtain bipolar coordinates and elliptic coordinates. First, we consider the mapping of $z = i\cot(\frac{w}{2})$ with

$$x = \frac{\sinh v}{\cosh v - \cos u}, \tag{3}$$

$$y = \frac{\sin u}{\cosh v - \cos u}, \tag{4}$$

which is usually used for bipolar coordinates. The inverse mapping is $w = 2\cot^{-1}[\frac{z}{i}]$ with

$$v(x, y) = \cosh^{-1}\left(\frac{x^2 + y^2 + 1}{\sqrt{(x^2 + y^2 + 1)^2 - 4x^2}}\right), \tag{5}$$

[$u(x, y)$ is not shown here]. Now we suppose to apply the Mikaelian lens $n_w = \frac{1}{\cosh(mv)}$, under the above mapping, it is very easy to obtain the profile in z space:

$$n_z = \frac{1}{\cosh(mv)}\frac{2}{|z^2 - 1|} = \frac{1}{\cosh[mv(x, y)]}\frac{2}{\sqrt{(x^2 + y^2 + 1)^2 - 4x^2}}, \tag{6}$$

which we shall call the bipolar Maxwell's fish-eye lens.

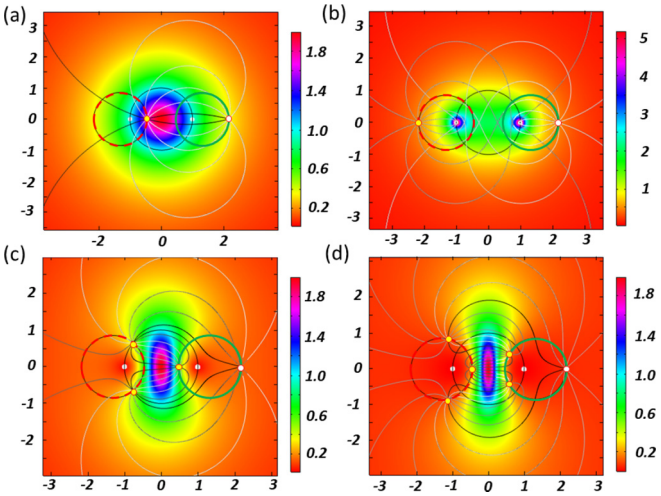

FIG. 3. The ray trajectories and refractive index profiles for a bipolar Maxwell's fish-eye lens with (a) $m = 1$, (b) $m = 1/2$, (c) $m = 2$, and (d) $m = 3$. The white points are the sources while the yellow points are images. The solid circles in green are mapped from the line $v = +1$, while the dashed circles in red are mapped from the line $v = -1$.

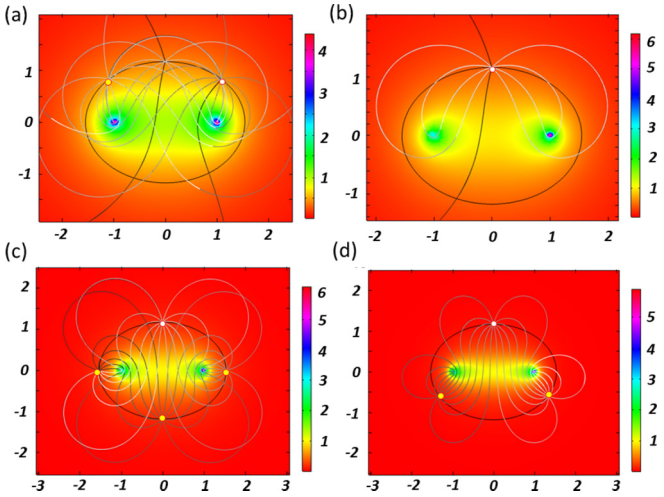

FIG. 4. The ray trajectories and refractive index profiles for an elliptic Maxwell's fish-eye lens with $m = 1$ for the source at (a) $(\cosh 1 \cos \frac{\pi}{4}, \sinh 1 \sin \frac{\pi}{4})$ and (b) $(0, \sinh 1)$, and with (c) $m = 2$ and (d) $m = 3$ for the source at $(0, \sinh 1)$. The white points are the sources while the yellow points are images.

For $m = 1$, it will come back to the form of Maxwell's fish-eye lens $n_z = \frac{2}{x^2+y^2+1}$. For bipolar coordinates, any fix u or v are related to two orthogonal sets of circles. For $v = \pm 1$, they are related to two circles: $(x \mp \coth 1)^2 + y^2 = \frac{1}{\sinh^2 1}$. According to the imaging principle of Mikaelian lens, any source at each circle will cause images or self-images at these two circles. For example, we plot the ray trajectories for this mapping for $m = 1$ (i.e., Maxwell's fish-eye lens), and the related refractive index profile in Fig. 3(a). The source and self-image is at $(\coth 1 + \frac{1}{\sinh 1}, 0)$ and the image is at $(-\coth 1 + \frac{1}{\sinh 1}, 0)$. If $m = 1/2$, the trajectories are no longer circles, which are plotted together with the refractive index profile in Fig. 3(b). The maximum values of the refractive index are singular infinities and at $(1, 0)$ and $(-1, 0)$. The source and self-image is at $(\coth 1 + \frac{1}{\sinh 1}, 0)$ and the image is at $(-\coth 1 - \frac{1}{\sinh 1}, 0)$. Before the imaging, the trajectories travel around $(1, 0)$ and $(-1, 0)$ each time. There are also trajectories for self-imaging around each singularity, which is very similar to the generalized Maxwell's fish-eye lens with $m = 1/2$. If $m = 2$, the trajectories and the related refractive index profile are plot in Fig. 3(c), where the maximum values are at the origin. The source at $(\coth 1 + \frac{1}{\sinh 1}, 0)$ will cause another image at $(\coth 1 - \frac{1}{\sinh 1}, 0)$ at the right circle and two other images at the left circle before self-imaging. If $m = 3$, the trajectories and the related refractive index profile are plot in Fig. 3(d), which is similar to that in Fig. 3(c) but with a more concentrating region with higher indexes. The source at $(\coth 1 + \frac{1}{\sinh 1}, 0)$ will cause two images at the right circle and three other images at the left circle before self-imaging.

Second, we consider the mapping of $z = \cosh w$ with

$$x = \cosh u \cos v, \tag{7}$$

$$y = \sinh u \sin v, \tag{8}$$

which is usually used for elliptic coordinates. The inverse mapping is $w = \cosh^{-1} z$ with

$$u(x, y) = \cosh^{-1}\left(\sqrt{\frac{x^2+y^2+1+\sqrt{(x^2+y^2+1)^2-4x^2}}{2}}\right), \tag{9}$$

[$v(x, y)$ is not shown here]. Now we suppose to apply the Mikaelian lens $n_w = \frac{1}{\cosh(mu)}$, under the above mapping, we can obtain the profile in z space:

$$\begin{aligned} n_z &= \frac{1}{\cosh(mu)} \frac{1}{\sqrt{|z^2-1|}} \\ &= \frac{1}{\cosh[mu(x, y)]} \frac{1}{\sqrt{\sqrt{(x^2+y^2+1)^2-4x^2}}}, \end{aligned} \tag{10}$$

which we shall call the elliptic Maxwell's fish-eye lens. For elliptic coordinates, any fixed u are related to a set of ellipses, and any fixed v are related to a set of hyperbola, which are orthogonal to the ellipses. However, it is a bit different from the exponential mapping and the circular coordinates, where u ranges from $-\infty$ to $+\infty$. In this case, u ranges from 0 to $+\infty$. Hence, both $\pm u$ are related to one single ellipse. If we put a source at $(\cosh 1 \cos \frac{\pi}{4}, \sinh 1 \sin \frac{\pi}{4})$, it will form an image at $(\cosh 1 \cos \frac{3\pi}{4}, \sinh 1 \sin \frac{3\pi}{4})$ for $m = 1$, as shown in Fig. 4(a). The refractive index goes to infinity at both $(1, 0)$ and $(-1, 0)$. There are some trajectories going around $(1, 0)$ for self-imaging, while others travel around $(-1, 0)$ for imaging. If the source is at $(0, \sinh 1)$, the image overlaps with it, we then find self-imaging even with $m = 1$, as demonstrated in Fig. 4(b). For $m = 2$, we plot the ray trajectories and refractive index profile in Fig. 4(c), where the index goes to infinity as well at both $(1, 0)$ and $(-1, 0)$. For the source at $(0, \sinh 1)$, there will be images along the ellipse

at (cosh 1, 0), (0, −sinh 1), and (−cosh 1, 0), respectively. For $m = 3$, we also plot the ray trajectories and refractive index profile in Fig. 4(d). The profile is similar to those of $m = 1$ and $m = 2$. However, it seems there are only three images or self-images along the ellipse for the source at (0, sinh 1). This is due to the overlapped effect like that in Fig. 4(b). If we put the source at $(\cosh 1 \cos \frac{\pi}{4}, \sinh 1 \sin \frac{\pi}{4})$, there will be six images, like the circular case in Fig. 2(a).

In conclusion, we propose a method to construct new types of absolute instruments by combining the Mikaelian lens together with conformal mappings. There will be self-imaging and imaging effects along closed conformal curves. Such lenses will be very useful in conformal cloaking designs, especially to reduce their refractive index ranges for easy implementations. In addition, such a method can also be used to design other lenses with special imaging functionalities. For example, if the scaling parameter in Mikaelian lens is an irrational number, the imaging effect will be maintained along the curves forever while there will be no self-imaging effect, and thereby the lens is no longer an absolute instrument. If we choose other orthogonal directions for the Mikaelian lens, e.g., the radial directions, the hyperbolic directions, or the parabolic directions from parabolic coordinates, the imaging effect will precisely happen along those predesigned open curves. Hence our method is general for two dimensions and could be used on special waveguide design, microcavity design, and even cloaking designs in future. There are only several conformal mappings for three dimensions, which still needs further explorations on this aspect.

This work was supported by the National Science Foundation of China (Grant No. 11874311) and the Fundamental Research Funds for the Central Universities (Grant No. 20720170015).

[1] J. L. Synge, Trans. Amer. Math. Soc. **44**, 32 (1938).
[2] T. Tyc, L. Herzanova, M. Sarbort, and K. Bering, New J. Phys. **13**, 115004 (2011).
[3] U. Leonhardt and T. Philbin, *Geometry and Light: The Science of Invisibility* (Courier Corporation, Chelmsford, MA, 2012).
[4] L. Xu and H. Chen, Nat. Photon. **9**, 15 (2014).
[5] R. K. Luneburg, *Mathematical Theory of Optics* (University of California Press, Berkeley, CA, 1964).
[6] J. E. Eaton, Trans. IRE Antennas Propag. **4**, 66 (1952).
[7] J. C. Maxwell, Camb. Dublin Math. J. **8**, 188 (1854).
[8] C. Pfeiffer and A. Grbic, IEEE Trans. Antennas Propagat. **58**, 3055 (2010).
[9] U. Leonhardt, New J. Phys. **11**, 093040 (2009).
[10] U. Leonhardt, Science **312**, 1777 (2006).
[11] J. C. Minano, Opt. Express **14**, 9627 (2006).
[12] M. Sarbort and T. Tyc, J. Opt. **14**, 075705 (2012).
[13] T. Tyc and A. J. Danner, Phys. Rev. A **96**, 053838 (2017).
[14] A. Danner, H. L. Dao, and T. Tyc, Opt. Express **23**, 5716 (2015).
[15] J. B. Pendry, D. Schurig, and D. R. Smith, Science **312**, 1780 (2006).
[16] H. Chen, C. T. Chan, and P. Sheng, Nat. Mater. **9**, 387 (2010).
[17] D. Schurig, J. Mock, B. Justice, S. A. Cummer, J. B. Pendry, A. Starr, and D. Smith, Science **314**, 977 (2006).
[18] Y. G. Ma, C. K. Ong, T. Tyc, and U. Leonhardt, Nat. Mater. **8**, 639 (2009).
[19] N. Kundtz and D. R. Smith, Nat. Mater. **9**, 129 (2010).
[20] A. Mikaelian and A. Prokhorov, Progress in Optics **17**, 279 (1980).
[21] X. Wang, H. Y. Chen, H. Liu, L. Xu, C. Sheng, and S. Zhu, Phys. Rev. Lett. **119**, 033902 (2017).